Renewable Energy 239 (2025) 121979

Contents lists available at ScienceDirect

Renewable Energy

journal homepage: www.elsevier.com/locate/renene

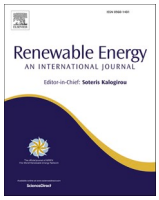

Enhancing radiative sky cooling performance by employing crossed compound parabolic concentrating configurations

Ya Dan [a], Mingke Hu [b,*], Qiliang Wang [a], Yuehong Su [a,**], Saffa Riffat [a]

[a] Department of Architecture and Built Environment, The University of Nottingham, Nottingham, NG7 2RD, United Kingdom
[b] School of Mechanical Engineering, Southwest Jiaotong University, Chengdu, 610031, China

ARTICLE INFO

Keywords:
Crossed compound parabolic concentrator
Radiative cooling
Spectral property
Cooling power density
Solar acceptance ratio

ABSTRACT

Achieving superior radiative sky cooling (RC) performance in practical applications is challenging due to its cooling power is easily compromised by unwanted thermal energy influxes, including solar heat gain and thermal radiation from nearby warm objects. To address this issue, the present work introduces the integration of affiliated crossed compound parabolic concentrators (CPC) as a means to effectively mitigate this thermal burden. Through the development of a comprehensive mathematical framework that characterizes the heat exchange between the RC emitter and different environmental heat sources, the cooling performance of the novel crossed CPC-RC module is evaluated and compared with other RC configurations. The results show that due to its excellent capability to shield unfavourable heat inflows from large zenith angles, the crossed CPC-RC module shows the potential to reach a cooling power density of 99.50 W/m^2 at noon, outperforming the flat-RC and 2D CPC-RC modules by 5.1% and 41.7%, respectively. Furthermore, key parameters optimization and the cooling performance assessment throughout a typical summer day is carried out to demonstrate the superiority of the crossed CPC structure in boosting cooling capacity, particularly the cooling benefits throughout the day, thereby offering a promising solution to better align with the cooling demands of buildings.

1. Introduction

The rapid development of modern society has resulted in a substantial rise in energy consumption, consequently driving a significant increase in carbon emissions [1]. Furthermore, as morethan 80% of the primary energy supply continues to depend on non-renewable sources such as fossil fuels [2], this reliance has further aggravated issues of energy shortages and environmental pollution [3–5]. Consequently, the advancement and research of renewable and environmentally friendly energy technologies have become a critical priority [6,7]. Among them, radiative sky cooling (RC) technology, which harnesses natural cold sources from outer space, is considered an attractive passive cooling approach. It utilizes the "atmospheric window" in the 8–13 μm wavelength range to emit thermal infrared radiation to the deep universe (~3 K), thereby enabling self-cooling with significant application prospects [8–11]. However, as depicted in Fig. 1, the cooling power density (P_{cool}) for the RC module not only depends on the thermal radiation flux emitted by the RC emitter (P_{emi}) but also by the thermal radiation absorbed from the sky (P_{sky}) and surroundings (P_{sur}). Moreover, the most significant impact on its cooling performance is the absorbed solar radiation (P_{sol}). Although solar radiation has unlimited potential for solar applications and is uniformly available everywhere [12], typically reaching an intensity of around 1000 W/m^2 on a sunny day, this value significantly surpasses the cooling flux generated by RC modules at ambient temperature, which is approximately 100 W/m^2 [13]. This substantial discrepancy underscores the challenges of utilizing RC technology to achieve effective daytime cooling.

Nomenclature

C	Concentration ratio of concentrator
f	focal length of the CPC
G	Total incident solar radiation, W/m^2
H	Height of crossed CPC-RC modules, mm
h	Convection heat transfer coefficient, W·m^{-2}·K
i	Number of reflections
I_b	Blackbody spectral intensity, W·m^{-2}·μm^{-1}·sr^{-1}
P	Power density, W/m^2

(*continued on next page*)

* Corresponding author.
** Corresponding author.
E-mail addresses: mingke.hu@swjtu.edu.cn (M. Hu), yuehong.su@nottingham.ac.uk (Y. Su).

https://doi.org/10.1016/j.renene.2024.121979
Received 7 September 2024; Received in revised form 8 November 2024; Accepted 21 November 2024
Available online 22 November 2024

(*continued*)

T	Temperature, K or °C
W	Width of the RC emitter, mm
Greek symbols	
α	Absorptivity
β	Respective ratios of the radiation beam, %
ε	Emissivity
ρ	Reflectivity
η	Solar acceptance ratio, %
λ	Wavelength, μm
ω	Radiation beam ratio, %
θ_{max}	Maximum half-acceptance angle of CPC
θ	Zenith angle, °
φ	Azimuth angle, °
σ	Stefan-Boltzmann constant, $W{\cdot}m^{-2}{\cdot}K^{-4}$
Subscripts	
amb	Ambient
con	Concentrator
con+cov	Heat conduction and convection
cool	Cooling
eff	Effective
emi	Emitter
env	External environment
gro	Ground
sol	Solar radiation
sur	Aboveground surroundings

Advances in materials science have enabled researchers to develop RC materials with near-ideal spectral properties [14], characterized by extremely low absorptivity in the solar spectrum while maintaining high emissivity in the infrared region [15]. These materials have the potential to achieve sub-ambient cooling throughout the day [16–19]. However, further improvements in the spectral selectivity of near-ideal RC materials face challenges. Additionally, they are unable to ensure high-quality cooling in complex real-world environments, where the impacts of external environmental thermal radiation and solar radiation absorbed by the RC modules cannot be mitigated [20]. Consequently, further research is necessary to optimize the structural design of the RC module and enhance its ability to block solar and external environmental thermal radiation. Currently, several researchers have proposed novel systems that combine RC modules with external shielding structures. For example, utilizing cone-shaped shields [21,22], reflective troughs [23], V-shaped spectrally selective mirrors [24], and other configurations [25,26] can effectively shield against adverse thermal radiation from large zenith angles and non-radiative heat exchange, achieving excellent cooling effect. In addition, combining concentrators commonly used in solar energy utilization with RC technology to form a concentrated RC system [27] can also enhance cooling performance.

In this context, an RC module based on a two-dimensional compound parabolic concentrator (2D CPC-RC module) was developed and studied by the authors in a previous work [28]. Nighttime experiments conducted in Nottingham, UK demonstrated its superior cooling performance, which was more than 30% higher than that of conventional flat-RC modules. However, daytime experiments in summer revealed that the horizontally placed module struggled to reach sub-ambient temperatures This limitation arises because the CPC structure cannot block solar radiation with an incident angle smaller than the maximum half-acceptance angle (θ_{max}) of the CPC [29]. Furthermore, due to its concentrating properties, some solar radiation that would not typically reach the flat-RC module is redirected to the RC emitter [30]. However, due to the constantly changing trajectory of the sun, when the solar incident angle exceeds the maximum acceptance angle (θ_{max}) of the CPC, the unshaded side of the CPC is unable to effectively block solar radiation in the morning or afternoon. As illustrated in Fig. 2, a portion of solar radiation can still enter the 2D CPC-RC module through the side openings (indicated by the pink areas). Additionally, when obstacles are present in the surroundings, substantial thermal radiation from the external environment can also penetrate through these side openings, further diminishing the cooling performance of the module.

In order to reduce the absorption of adverse solar radiation by RC modules and thereby improve their cooling capacity throughout the day, this study proposes a novel concentrated RC module integrating with a four-sided closed-crossed CPC structure, referred to as the crossed CPC-RC module, as shown in Fig. 2. The crossed CPC structure, commonly used in solar energy collection systems, consists of two 2D CPCs and exhibits excellent optical efficiency [31,32]. When applied to RC systems, this structure utilizes reflectors to prevent the thermal radiation emitted by the RC emitter from escaping through the side openings, concentrating the emitted thermal radiation into a narrower hemispherical range. However, since the structure is based on the 2D CPC, its concentration characteristic is similar, meaning its height varies with different concentration ratios (C) [33]. A higher C results in the RC module collecting more solar radiation when the solar incident angle is less than its θ_{max}. However, once the solar incident angle exceeds θ_{max} of crossed CPC, the structure becomes more effective at blocking solar radiation from large incident angles. Therefore, it is crucial to evaluate the cooling performance of the crossed CPC-RC module across different configurations to achieve optimal results. Additionally, when the RC module is situated in a complex external environment, such as when many obstacles surround the RC module or when the module is positioned on an inclined plane., the crossed CPC structure effectively shields the thermal radiation from the surrounding obstacles and the

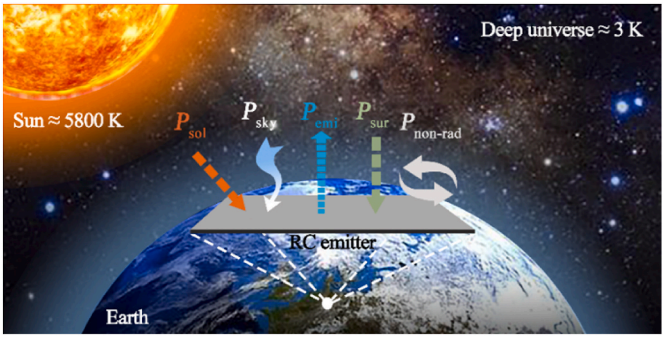

Fig. 1. Schematic diagram of heat transfer processes on a radiative cooling emitter.

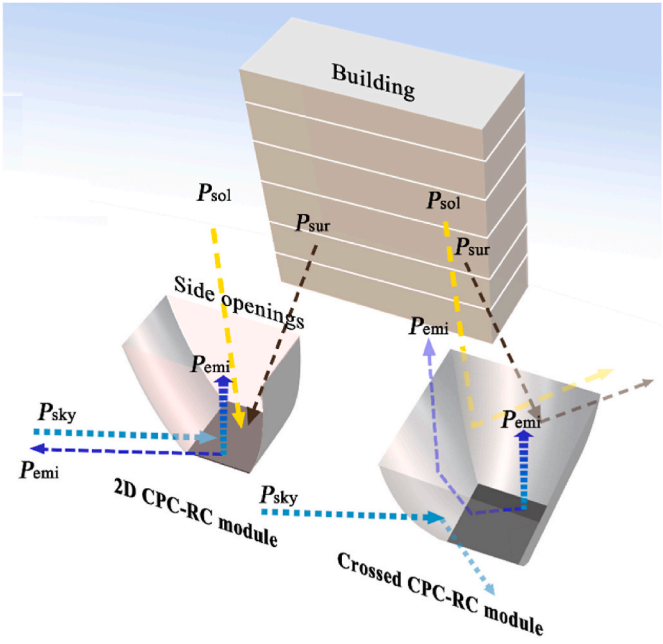

Fig. 2. Difference between 2D CPC-RC and crossed CPC-RC modules in shielding solar and other adverse thermal radiation.

ground, preventing it from entering the RC module through the side openings.

In this paper, the cooling performance of the novel crossed CPC-RC module, along with other two concentrated RC modules and a flat-RC module is accurately evaluated, demonstrating the effectiveness of the crossed CPC-RC module in shielding undesirable thermal radiation and solar radiation from large zenith angles. Besides, the cooling performance of crossed CPC-RC modules under different CPC configurations (varying concentration ratios) is analysed. Finally, due to the high sensitivity of concentrated RC modules to solar radiation, the cooling performance and average hourly cooling power throughout a typical summer day for different RC modules are examined. The development of this innovative RC module provides new ideas for the wider application of RC technology in practical applications, showing its great potential in improving cooling efficiency and environmental adaptability.

2. Module description

The radiative heat exchange schematic diagram between the 2D CPC-RC module and the crossed CPC-RC module with the sun and external environment is illustrated in Fig. 3 (a). The crossed CPC structure comprises of four parabolic surfaces and a square aperture [34]. When the 2D CPC-RC module's side openings are aligned along the east-west direction, P_{sol} from the morning and evening, along with P_{sky} from the east or west, can reach the RC emitter of the 2D CPC-RC module through side openings. In contrast, such thermal radiations are effectively blocked by the wing frameworks of the crossed CPC structure, thereby enhancing its cooling performance.

However, in low-latitude areas, the solar altitude angle is relatively high in summer, especially at noon when the sun is around the zenith direction. In this situation, the concentrators of the CPC-RC modules cannot function as solar shields, instead, they concentrate solar radiation onto the RC emitter, thereby increasing the difficulty of daytime cooling. Therefore, in CPC-RC modules, the solar radiation absorbed at different times or during different seasons is a critical evaluation indicator. This paper introduces the solar acceptance ratio (η_{con}) to represent the ratio of solar radiation reaching the RC emitter to the solar radiation reaching the CPC-RC module aperture. The module aperture is depicted in the blue area of Fig. 3 (b). For CPC-RC modules, a larger η_{con} indicates that more solar radiation is reaching the RC emitter, causing the module's P_{sol} to increase and obtaining a lower P_{cool}. In addition to the η_{con}, investigating the P_{env} for the crossed CPC-RC and 2D CPC-RC modules reveals that different CPC configurations vary in their effectiveness at blocking external environmental thermal radiation from reaching the RC emitter. This analysis allows for identifying the CPC configuration that achieves excellent RC effect. Furthermore, variations in environmental parameters and RC material properties influence cooling performance. Consequently, this study focuses on the cooling performance of the crossed CPC-RC modules with different configurations under varying parameters.

As a numerical analysis paper, all concentrator materials in this paper utilized specular aluminium, with reflectivity as high as 0.95 across the entire wavelength range [35]. Additionally, when setting the spectral characteristics of the RC emitter, considering that the influence of α_{sol} on the daytime cooling effect is greater than that of ε_{emi}, α_{sol} is used as the key parameter for comparison in the following sections and will be discussed in detail. For the ε_{emi} setting of the RC emitter, this paper employs a spectrally selective RC emitter, as illustrated in Fig. 4. The RC emitter has a weighted average emissivity of 0.95 within the "atmospheric window," while its emissivity in other infrared regions is set to 0.

3. Modelling approach

3.1. Mathematical model

In this study, a previously established modelling approach is used to quantitatively assess the net cooling power density (P_{cool}) for the crossed CPC-RC module and other RC modules under varying parameters. The numerical analysis relies on specific assumptions to formulate equations describing the heat transfer between the RC module and the external environment. Furthermore, the emitter temperature (T_{emi}) is consistently set equal to the ambient temperature (T_{amb}), allowing the non-radiative heat transfer ($P_{non\text{-}rad}$) between the RC module and its surroundings to be disregarded.

In this modelling approach, the thermal radiation from the sky, ground and surrounding environment is attributed to the thermal radiation from the external environment, so the P_{cool} obtained by the RC

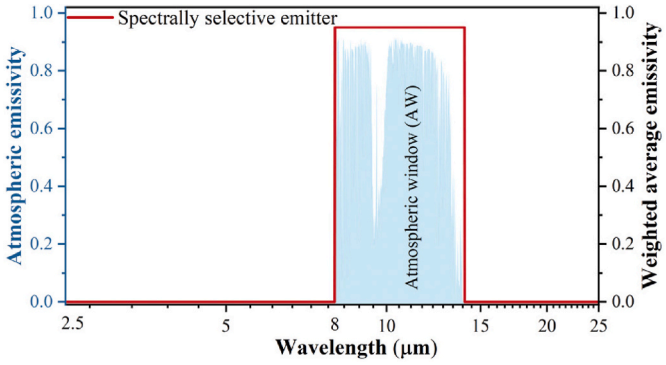

Fig. 4. Average emissivity of spectrally selective emitter across 2.5–25 μm.

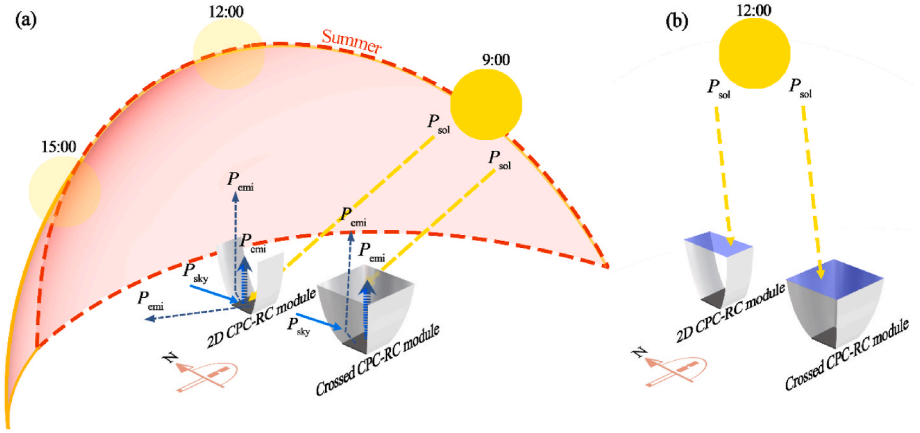

Fig. 3. (a) Radiative heat exchange between 2D CPC-RC and crossed CPC-RC modules and external environment. (b) Definition of solar acceptance ratio.

modules can be expressed as:

$$P_{cool} = P_{emi} - \left(P_{sky} + P_{gro} + P_{sur}\right) P_{env} - P_{sol} - P_{con+cov} \quad (1)$$

Based on the above assumption, $P_{con+cov}$ are considered to be neglective, and therefore will not be mentioned in the following discussions.

3.1.1. Radiation power emitted by the RC emitter

The thermal radiation emitted by the RC emitter is solely influenced by its intrinsic spectral characteristics, unaffected by the external environment, which can be expressed as follows [26]:

$$P_{emi} = \int_0^{\infty} \int_0^{2\pi} \int_0^{\pi/2} \varepsilon_{emi}(\theta, \varphi, \lambda) I_b(\lambda, T_{emi}) \cos\theta \sin\theta d\theta d\varphi d\lambda \quad (2)$$

where $\varepsilon_{emi}(\theta, \varphi, \lambda)$ is the spectral, directional emissivity of the emitter, $I_b(\lambda, T_{emi})$ is the blackbody spectral intensity at the T_{emi}, $W{\cdot}m^{-2}{\cdot}\mu m^{-1}{\cdot}sr^{-1}$. According to the Stefan-Boltzmann law, Eq. (2) can be simplified as [36]:

$$P_{emi} = \varepsilon_{emi} \sigma T_{emi}^4 \quad (3)$$

where ε_{emi} is the total, hemispherical emissivity of the RC emitter; and σ is the Stefan-Boltzmann constant, 5.67×10^{-8} $W{\cdot}m^{-2}{\cdot}K^{-4}$.

3.1.2. External environmental radiation power absorbed by the RC emitter

The thermal radiation absorbed by the RC module from the entire external environment as a new parameter proposed in previous study, which can be expressed as [37]:

$$P_{env} = \int_0^{\pi/2} \int_0^{2\pi} \int_0^{\infty} \alpha_{emi}(\theta, \varphi, \lambda) \varepsilon_{env}(\theta, \varphi, \lambda) I_b(\lambda, T_{amb}) \cos\theta \sin\theta d\lambda d\varphi d\theta \quad (4)$$

where $\alpha_{emi}(\theta, \varphi, \lambda)$ is the spectral, directional absorptivity of the emitter; $\varepsilon_{env}(\theta, \varphi, \lambda)$ represents the overall spectral, directional emissivity of the external environment. This parameter represents the weighted average of the equivalent sky, ground, and aboveground surroundings emissivity. A detailed explanation of the parameters can be found in Ref. [38]. As this study assumes that the RC module is positioned horizontally, thermal radiation from the ground does not reach the RC emitter and will be excluded from the subsequent calculations.

It is important to note that, similar to the equivalent sky emissivity, the terms $\varepsilon_{sur}(\theta, \varphi, \lambda)$ in Eq. (4) do not represent the real emissivity but instead denote the equivalent emissivity of the aboveground surroundings at ambient temperature T_{amb}, can be expressed as

$$\varepsilon_{sur}(\theta, \varphi, \lambda) = \frac{\varepsilon'_{sur}(\theta, \varphi, \lambda) T_{sur}^4(\theta, \varphi)}{T_{amb}^4} \quad (5)$$

where $\varepsilon'_{sur}(\theta, \varphi, \lambda)$ is the real spectral emissivity of the aboveground surroundings at the direction (θ, φ) relative to the RC emitter; and $T_{sur}(\theta, \varphi)$ denotes the temperature of the aboveground surroundings at the direction (θ, φ) relative to the RC emitter, K.

Furthermore, as in Eq. (3), P_{env} can be simplified to:

$$P_{env} = \alpha_{emi} \varepsilon_{env} \sigma T_{amb}^4 \quad (6)$$

where α_{emi} is the total, hemispherical absorptivity of the RC emitter; ε_{env} is the equivalent external environmental emissivity. Using the modelling approach for simulation and derivation, ε_{env} can be expressed as [38]:

$$\varepsilon_{env} = \int_0^{\pi/2} \left[\varepsilon_{env}(\theta) \beta_{env}(\theta) \left(\sum_{i=0}^{+\infty} \rho_{con}^i \omega_i(\theta) \right) \rho_{con\_eff} \right] d\theta \quad (7)$$

where $\varepsilon_{env}(\theta)$ is the equivalent emissivity of the whole external environment in the zenith angle of θ; $\beta_{env}(\theta)$ is the ratio of the radiation beam falling on the ring formed by the zenith angle θ between the incident direction and the zenith direction relative to the total, hemispheric radiation beam of the RC emitter, as shown in blue lines in Fig. 5. The method of obtaining $\beta_{env}(\theta)$ has been explained in detail in Ref. [37]. ρ_{con_eff} is the effective reflectivity for the concentrators to the thermal radiation from the external environment. For non-concentrated RC modules, the ρ_{con_eff} is 1; i represents the number of reflections by the concentrators required for thermal radiation to reach the RC emitter; ρ_{con} is the real material reflectivity of the concentrators; $\omega_i(\theta)$ represents the ratio of the number of incoming radiation beams from the same zenith angle θ that reach the RC module after i-time reflections to the total radiation beams. The approach of determining this parameter is described in detail in Ref. [38].

3.1.3. Solar irradiation absorbed by the RC emitter

The solar radiation power absorbed by the RC modules plays a key role in whether sub-ambient cooling effect can be achieved during the daytime, which can be expressed as:

$$P_{sol} = \alpha_{emi} G_{sol} \quad (8)$$

For concentrated RC modules, the absorbed solar radiation must be redefined to account for the concentrating effect, and it can be expressed as:

$$P_{sol} = C \eta_{con} \alpha_{emi} G_{sol} \rho_{con\_sol} \quad (9)$$

where C is the concentration ratio of the concentrator; η_{con} is the solar acceptance ratio of the concentrated RC module; G_{sol} is the total incident solar radiation, W/m^2; ρ_{con_sol} represents the effective reflectivity of the CPC to solar radiation, which in this study is set equal to the reflectivity of the material itself.

3.2. Simulation model setting and analysis

In this study, Rhino software is utilized to create an accurate model of the RC module, while the optical software Photopia [39] is employed to assign specific material properties to the model. The detailed modelling process has been described in Ref. [37]. Therefore, this section provides only a brief overview of the method's principles. First, by setting the sunlight from different incident angles and running the simulation, the total radiative flux obtained from the module aperture and the RC emitter is determined to obtain the module's η_{con}. Furthermore, based on the principle of reciprocity, a uniform diffuse lamp

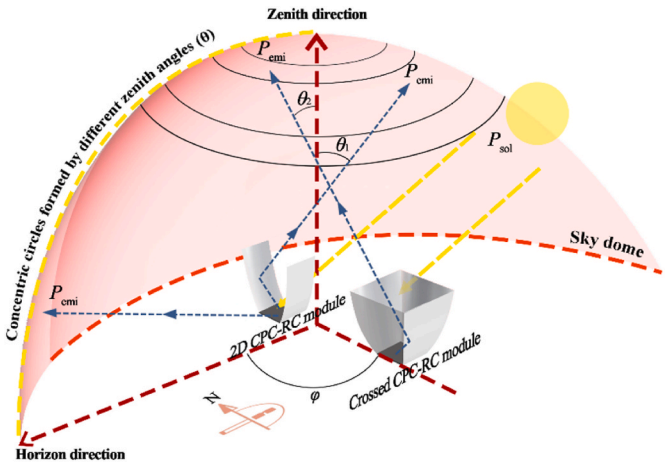

Fig. 5. Schematic diagram of the directional radiation beam emitted by the RC emitter.

replaces the RC emitter to emit radiations outward to characterize the radiation beam emitted by the RC emitter. The external environment is represented as a hemispheric black body, divided into 90 concentric rings via the zenith angle between the incident direction and the zenith direction, ranging from 0° (zenith direction) to 90° (parallel to the horizon). As the RC emitter uniformly emits radiation outward, the radiation beams passing through the different concentric rings are observed. The amount of radiation beams for each concentric ring is then divided by the total radiation beams to calculate $\beta_{env}(\theta)$ at various zenith angles.

4. Results and discussion

Based on the modelling approach, Section 1 analyses the cooling performance of four RC modules at various ambient temperatures, highlighting the superior nighttime cooling capability of the crossed CPC-RC module. Additionally, the 24-h cooling power on a typical summer day is examined. Section 2 investigates the variation in cooling power of the crossed CPC-RC modules at different concentration ratios (C) under different solar incidence angles and ambient temperatures (T_{amb}). Furthermore, the aboveground surrounding is set a concrete high-rise building occupying 10% of the whole external environment. The key parameter settings for the case study are provided in Table 1.

4.1. Cooling performance comparison for the different RC modules

This section first characterizes the nighttime absorbed P_{env} and obtained P_{cool} for four different RC modules at various T_{amb}, demonstrating the excellent adverse thermal radiation shielding effect of the crossed concentrator structures. Additionally, Section 4.1.2 examines variations in solar radiation (G_{sol}) and the solar absorptivity (α_{sol}) of the RC emitter affect the cooling performance of the RC module on a typical summer day in Guangzhou, China, further exploring the crossed concentrator structure's effectiveness in blocking solar radiation during the daytime.

Fig. 6 presents a schematic diagram of the four RC modules evaluated in this section, including a flat-RC module, a 2D CPC-RC module, a crossed inverted trapezoidal-RC module (referred to as the crossed "V"-RC module), and a crossed CPC-RC module. All four RC modules feature emitters with a uniform width (W) of 20 mm. Additionally, the height of the three concentrated RC modules is the same, each measuring 40 mm, which means that part of the concentrators is truncated in three concentrated RC modules. Finally, the three concentrated RC modules share the same C of 2x.

4.1.1. Effect of different ambient temperatures

To characterize the P_{env} and P_{cool} for the four RC modules, it is necessary first to obtain their ε_{env}. Since there is a fixed obstacle around the RC module in this paper, the emissivity of the equivalent sky and aboveground surroundings needs to be considered simultaneously when characterizing ε_{env}. Specifically, due to lacking a concentrator, the flat-RC module exhibits the highest ε_{env} at 0.718, indicating that it will absorb more external environmental thermal radiation. Furthermore, the concentrated RC modules with 2D and crossed structures demonstrate varying ε_{env} due to their structure differences. The 2D CPC-RC module absorbs more thermal radiation through the side openings, especially from the surrounding obstacle, resulting in a higher ε_{env} of 0.682. However, this portion of the thermal radiation can be blocked by the crossed concentrators in the crossed-structure RC modules. Consequently, the ε_{env} for the crossed "V"-RC and crossed CPC-RC modules is lower, at 0.654 and 0.639, respectively.

Table 1
Key parameter settings for case study.

Parameters	Descriptions	Values
T_{sur_night}	Nighttime surrounding temperature (°C)	$= T_{amb}$ [40]
T_{sur_day}	Daytime surrounding temperature (°C)	$T_{amb}+(\varepsilon_{sur}G_{sol})/h_{sur}$ [40]
h_{sur}	Surrounding convection heat transfer coefficient	25 W/m^2·K [41]
ε_{sur}	Surrounding emissivity	0.85 [42]
ρ_{con}	Concentrator material's reflectivity	0.95 [35]

Fig. 7 (a) shows P_{env} and P_{cool} for the four RC modules at different T_{amb} during the nighttime. According to the parameters provided in Table 1, the T_{sur} at night is assumed to be equal to the T_{amb}. The results indicate that across various T_{amb}, the P_{env} for the crossed CPC-RC module is the smallest among the four modules, while the P_{env} for the flat-RC module shows the largest. For example, when T_{amb} is 30 °C, the P_{env} for the crossed CPC-RC module is 288.42 W/m^2, which is 38.21 W/m^2 lower than that of the flat-RC module, demonstrating that the crossed CPC structure blocks 11.7% external environmental thermal radiation for the RC emitter. Similarly, the crossed CPC structure blocks 7.0% more external environmental thermal radiation than the 2D CPC structure. Fig. 7 (b) shows the P_{cool} for the four RC modules at different T_{amb}. The results indicate that the P_{cool} for the flat-RC module at various T_{amb} is significantly lower than that of the concentrated RC modules. Among the four RC modules, the crossed CPC-RC module achieves the highest P_{cool} due to its smaller P_{env}, followed by the crossed "V"-RC module and the 2D CPC-RC module. Specifically, at an T_{amb} of 0 °C, the crossed CPC-RC module demonstrates a cooling performance that is 83.9% and 12.6% higher than that of the flat-RC and 2D CPC-RC modules, respectively. When the T_{amb} increases to 40 °C, its P_{cool} is 10.36 and 21.25 W/m^2 larger than that of the crossed "V"-RC and 2D CPC-RC modules, respectively. These results highlight the crossed CPC-RC module' s excellent cooling capabilities during the nighttime.

4.1.2. 24-H cooling performance

This section examines the variations in hourly cooling power of four RC modules on 21st June, aiming to explore the differences in cooling performance under varying G_{sol} and T_{amb} conditions. Additionally, the impact of using different RC emitters on the daytime cooling performance of the RC module is investigated. Table 2 provides η_{con} for the three concentrated RC modules from 7:00 to 18:00 on 21st June. Since the 2D CPC-RC module allows solar radiation to reach the RC emitter through the side openings in the morning and evening, its η_{con} is not 0 between 7:00–8:00 and 16:00–18:00. Especially at 8:00 and 16:00, it reaches approximately 0.8, causing the module to absorb more solar radiation. In contrast, the crossed-structure RC modules can block solar radiation at certain times due to its four sides concentrator, resulting in η_{con} of 0 between 7:00–8:00 and 16:00–18:00. Additionally, at 9:00 and 15:00, the η_{con} for the 2D CPC-RC module is 0.95 and 0.92, respectively, while that of the crossed CPC-RC module is 0.60 and 0.61, as the solar altitude angle at these times is still lower than the crossed CPC-RC module's θ_{max}. However, during 10:00 to 14:00, the η_{con} for the three CPC-RC modules shows high values, which is not conducive to cooling capacity.

Compared to the flat-RC module, concentrated RC modules are influenced by the concentrating properties of the concentrator, which causes more solar radiation to be directed onto the RC emitter at specific times, thereby reducing the cooling effect of the RC modules during the daytime. Consequently, this study will focus on the variations in P_{sol} for the four RC modules as the sun's trajectory changes on 21st June. Additionally, daytime fluctuations in T_{amb} also influence T_{sur}, leading to variations in the thermal radiation emitted by surrounding obstacles. Fig. 8 presents the 24-h T_{amb} and G_{sol} on 21st June, along with the inferred T_{sur}. The weather data is provided from the EnergyPlus database.

Fig. 9 illustrates the P_{env} for four different RC modules on 21st June. The flat-RC module cannot block external environmental thermal radiation due to its lack of a concentrator, resulting in the highest P_{env} among the four RC modules, particularly during the daytime. This is attributed to the increase in T_{amb} during the daytime, which increases the emitted thermal radiation. Specifically, the P_{env} for the flat-RC module is 317.68 W/m^2 at 1:00, while at noon, P_{env} increases by

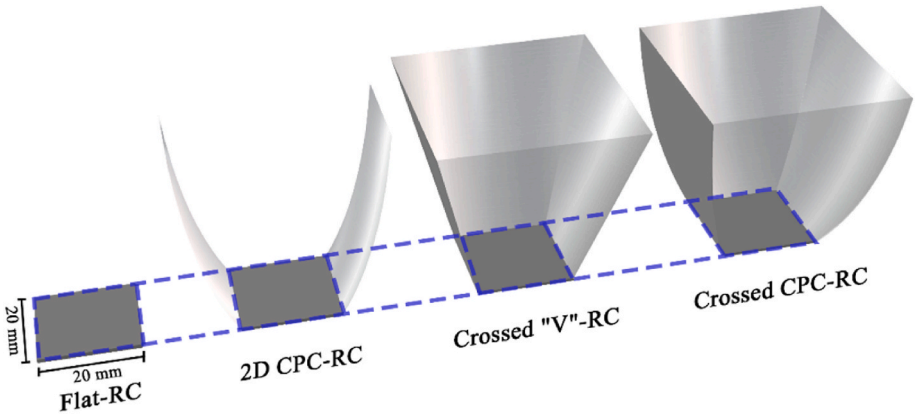

Fig. 6. Schematic diagram of the four compared RC modules.

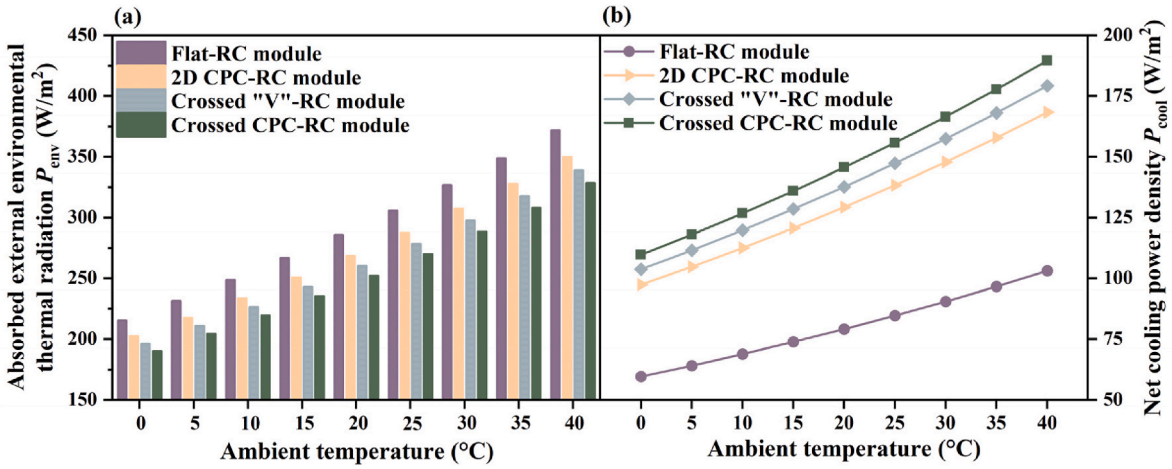

Fig. 7. (a) Absorbed external environmental thermal radiation and (b) obtained cooling power density for four RC modules at different ambient temperatures.

Table 2
Solar acceptance ratio for the three concentrated RC modules.

	7	8	9	10	11	12	13	14	15	16	17	18
2D CPC-RC	0.33	0.79	0.95	0.95	0.94	0.96	0.95	0.94	0.92	0.80	0.36	0.13
Crossed "V"	0	0	0.55	0.87	0.95	0.97	0.95	0.88	0.56	0	0	0
Crossed CPC	0	0	0.60	0.89	0.95	0.97	0.95	0.90	0.61	0	0	0

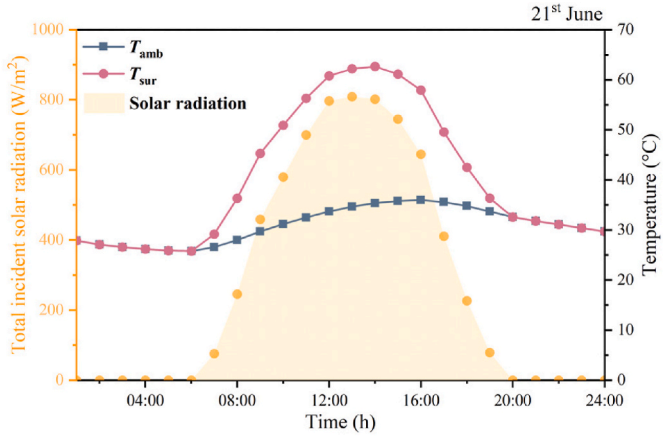

Fig. 8. Hourly total incident solar radiation, ambient and surrounding temperatures on 21st June.

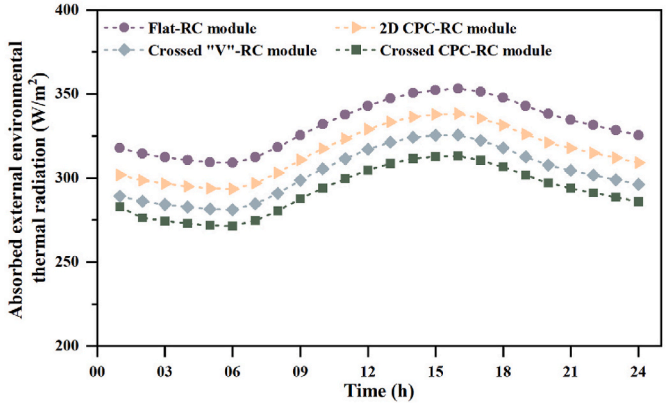

Fig. 9. Absorbed external environmental thermal radiation for the four RC modules on 21st June.

8.3%, which negatively impacts the RC effect. In contrast, the P_{env} for the other three RC modules with concentrator structures is consistently lower than that of the flat-RC module throughout the day. Notably, the crossed CPC-RC module shows P_{env} of 304.59 W/m^2 at noon, effectively blocking 11.2% of the adverse thermal radiation compared to the flat-RC module.

Fig. 10 shows the P_{cool} for the four RC modules on 21st June, with varying α_{sol} for the RC emitter. When α_{sol} is 0.05, the hourly P_{cool} for all RC modules exceed 70 W/m^2, even at noon. Among them, the flat-RC module has lower cooling performance during the nighttime compared to the other three concentrated RC modules due to the lack of concentrators. It obtains P_{cool} of 124.77 W/m^2, which is 8.8%, 18.6% and 21.8% lower than the 2D CPC-RC, crossed "V"-RC and crossed CPC-RC modules, respectively. However, during the daytime, its sensitivity to solar radiation is lower than the other three modules, resulting in a relatively stable P_{cool} curve. For instance, at 11:00, its P_{cool} is 97.57 W/m^2, while at 13:00, it exhibits 95.98 W/m^2, showing only a small difference. In contrast, the P_{cool} for the other three concentrated RC modules, especially the 2D CPC-RC module, drops sharply as solar radiation increases, from 117.35 W/m^2 at 8:00–87.33 W/m^2 at 10:00. Since the η_{con} for the crossed structure-RC module shows 0 between 7:00–8:00 and 16:00–18:00, their P_{cool} are higher than that of the 2D CPC-RC module during these periods. Between 9:00 and 15:00, the η_{con} for the three concentrators are similar, meaning their P_{sol} are also comparable. However, at noon, the P_{cool} for the crossed CPC-RC module reaches 99.50 W/m^2, which is 5.1% and 41.7% higher than that of the flat-RC and 2D CPC-RC modules, respectively. This improvement is due to the crossed CPC structure blocking adverse thermal radiation from entering the RC module through the side openings.

When α_{sol} increases to 0.10, the P_{cool} for the flat-RC module is higher than that of the other three concentrated RC modules around noon due to the concentrating characteristics of the concentrators. In contrast, for the 2D CPC-RC module, the hourly P_{cool} is lower than that of the flat-RC module from 8:00 to 16:00, totalling 9 h. This duration is reduced to 5 h for the crossed CPC-RC module. When α_{sol} is 0.15, the flat-RC module can still achieve a small cooling power at noon, while the 2D CPC-RC module cannot achieve any cooling effect between 10:00 and 3:00. The crossed structure-RC module performs slightly better but cannot provide cooling from 11:00 to 2:00. When α_{sol} increases to 0.20, even the flat-RC module fails to provide cooling effect around noon.

Fig. 11 illustrates the average hourly cooling power density ($\overline{P}_{cool}$) for the four RC modules on 21st June. By comparing this value, the cooling capacity of the RC modules throughout the day can be evaluated, providing a better reflection of each module's all-day cooling performance. The $\overline{P}_{cool}$ for all four RC modules decreases as the α_{sol} for the RC emitter increases. When α_{sol} is 0.05, the $\overline{P}_{cool}$ for the crossed CPC-RC module is 31.0% higher than that of the flat-RC module. The 2D CPC-RC module is significantly affected by adverse radiation, and its $\overline{P}_{cool}$ falls below that of the flat-RC module when α_{sol} exceeds 0.15. In contrast, due to the crossed CPC-RC module's effective thermal radiation shielding, it maintains $\overline{P}_{cool}$ for 102.76 W/m^2 even when α_{sol} increases to 0.2. This results in 27.56 W/m^2 more cooling power per hour than the flat-RC module and 49.30 W/m^2 higher than the 2D CPC-RC module.

This section first demonstrates the excellent nighttime cooling performance for the crossed CPC-RC module, attributed to its superior shielding against adverse thermal radiation (including the sky, surrounding obstacles, etc.), by comparing it with other traditional RC modules. When characterizing the cooling performance and average hourly cooling power for a typical summer day, it is observed that higher daytime ambient temperatures and solar radiation reduced the cooling

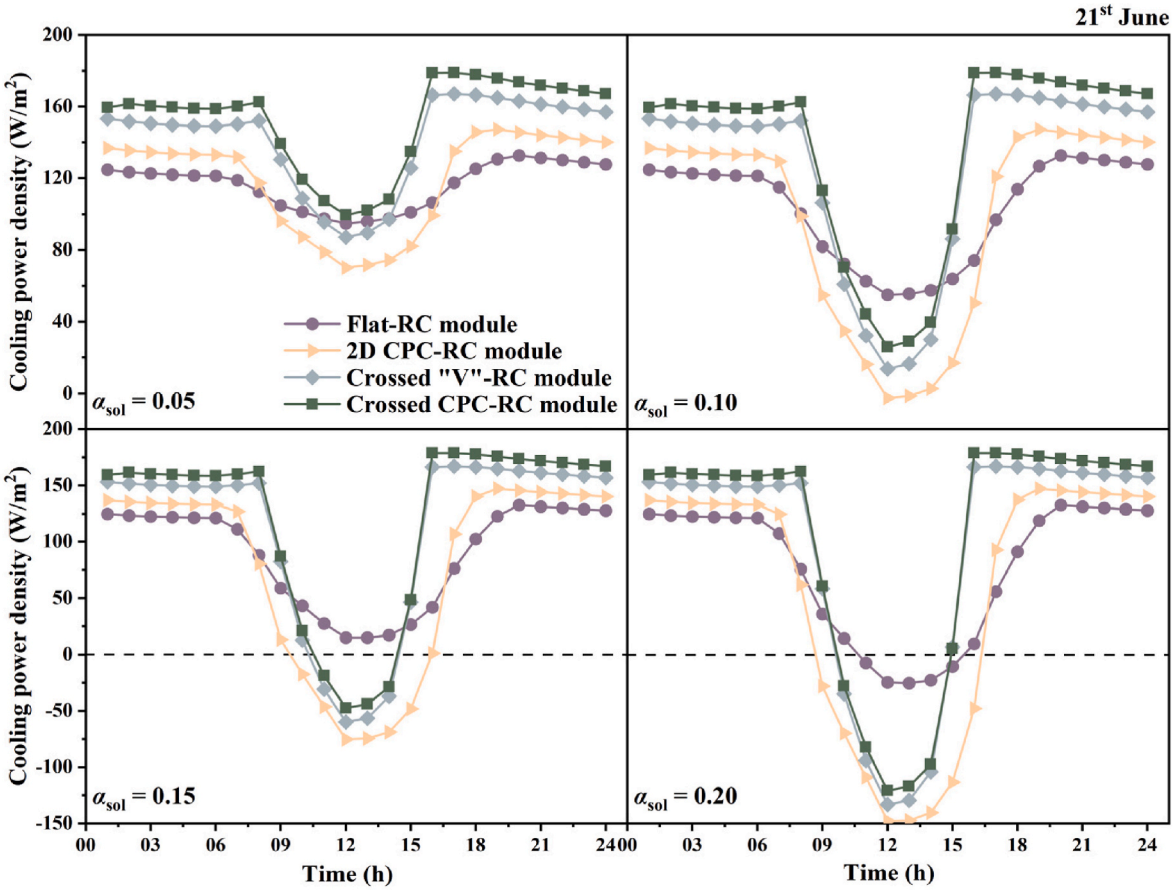

Fig. 10. Hourly cooling power density for the four RC modules with different RC emitters on 21st June.

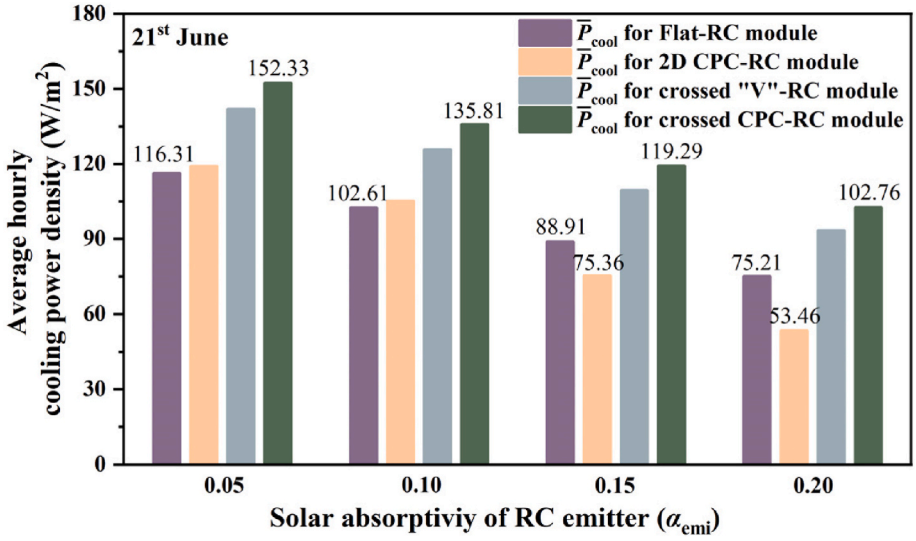

Fig. 11. Average hourly cooling power density for the four RC modules with different RC emitters on 21st June.

performance of RC modules. In addition, different solar absorptivity can also cause significant changes in the daytime cooling effect, especially for the 2D CPC-RC modules. In contrast, the crossed CPC structure offered additional shielding from solar radiation, thereby enhancing module's cooling performance throughout the day.

4.2. Cooling performance for the crossed CPC-RC modules with different configurations

In the previous section, the crossed CPC-RC module demonstrated the potential to achieve high-quality cooling power due to its four-sided shielding surfaces, which effectively block adverse thermal radiation and solar radiation from large zenith angles. However, further investigation is needed to assess the impact of the concentrator's concentration ratio (C) on RC performance. This section explores the effect of the variation of C in the crossed CPC structure on the absorption of solar radiation. Additionally, the P_{cool} for crossed CPC-RC modules with different configurations under varying T_{amb} and solar incident angles are also studied. Finally, the hourly P_{cool} and $\overline{P}_{cool}$ for the modules with different configurations on 21st June is evaluated. All crossed CPCs in this section are complete structures without truncation.

Fig. 12 shows three crossed CPC-RC modules with different C. Their bottom surfaces are set to square RC emitters with a width of 20 mm. As can be seen from the figure, the height of the crossed CPC structure (H) with different C is different. The larger the C, the higher the H. Furthermore, the parabola equation of the compound parabola can be expressed as:

$$y = \frac{1}{4f}x^2 \tag{10}$$

where f is the focal length of the CPC, which can be calculated by $f = W/2(\sin\theta_{max}+1)$. The θ_{max} can be determined based on the C.

4.2.1. Effect of solar incident angles

Fig. 13 illustrates the η_{con} for the crossed CPC-RC modules with different C at various solar incident angles. As the C increases, the θ_{max} of the crossed CPC structure decreases, causing the η_{con} to drop sharply when the solar incident angle exceeds the θ_{max}. When the C of the crossed CPC-RC module is 1.5x, the η_{con} at the solar incidence angle of 0–30° remains at a high level, exceeding 0.91. This indicates that larger part of solar radiation reaches the RC emitter within this incident angle range, which is not conducive to RC. When the solar incident angle exceeds 30°, surpassing the θ_{max} of the crossed CPC structure, η_{con} decreases rapidly, reaching 0 at 50°. Furthermore, when the C increases to 2x and 2.5x, the η_{con} at the incident angle of 30° drops to 0.47 and 0, respectively, indicating that the greater the C of the crossed CPC structures, the more solar radiation can be blocked.

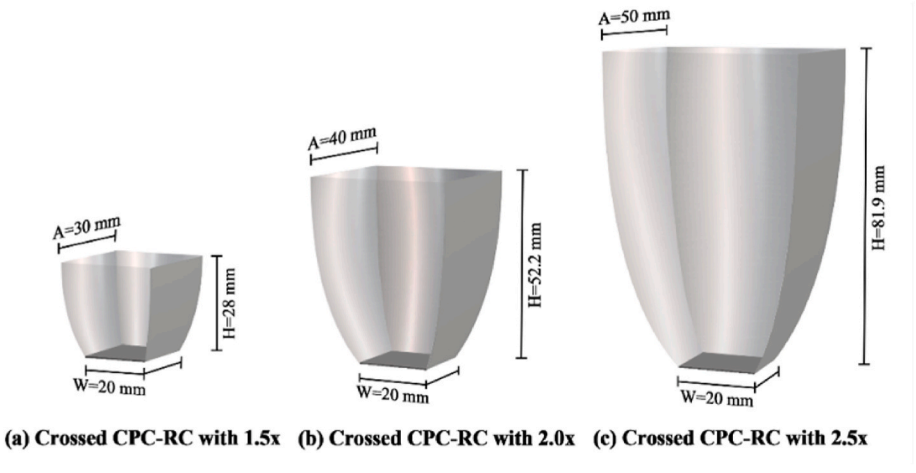

Fig. 12. Schematic diagram of three crossed CPC-RC modules with different concentration ratios.

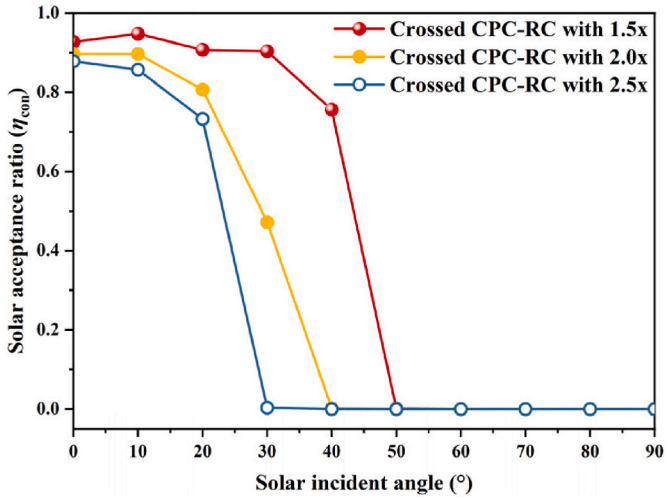

Fig. 13. Solar acceptance ratio for three crossed CPC-RC modules with different concentration ratios.

In addition to characterizing the η_{con} for crossed CPC-RC modules with different C, characterizing the ε_{env} for the module is also necessary. As C increases, the height of the crossed CPC increases, allowing more external environmental thermal radiation to be blocked by the structure, resulting in a decrease in ε_{env}. Specifically, the ε_{env} for the crossed CPC-RC module with 1.5x is 0.645, while the ε_{env} for RC modules with 2x and 2.5x is 0.639 and 0.626, respectively.

Fig. 14 (a) shows the variation of P_{cool} under different T_{amb} for the crossed CPC-RC modules with different C during both noon and nighttime, while Fig. 14(b) and (c) and (d) illustrates the effect on P_{cool} when the solar incident angle and T_{amb} change simultaneously during the daytime. Fig. 14 (a) indicates that during noon, regardless of T_{amb}, as the C of the crossed CPC-RC module increases, the P_{cool} for the RC module decreases, which is due to a larger C resulting in a higher P_{sol} for the module. For instance, when C is 1.5x, the P_{cool} for the crossed CPC-RC module at 0 °C is 50.85 W/m^2. However, when C increases to 2.5x, the P_{cool} drops to 26.55 W/m^2, which is 47.8% lower than the former. This difference diminishes as T_{amb} increases, when T_{amb} is 40 °C, the P_{cool} for the crossed CPC-RC module with 1.5x remains 17.5% higher than that of the crossed CPC-RC module with 2.5x. During the nighttime, without the influence of solar radiation, a larger C can reduce the view factor between the external environment and the RC emitter, thereby reducing the thermal radiation exchange and enhancing the cooling performance. When T_{amb} is 40 °C, the P_{cool} for the module with 2.5x reaches 193.73 W/m^2, which is 9.85 W/m^2 higher than that of the RC module with 1.5x.

Fig. 14 (b) shows that when C is 1.5x, the crossed CPC-RC module can still achieve a P_{cool} for 50.85 W/m^2 even when T_{amb} ia 0 °C at noon. However, the RC module exhibits a higher η_{con} at small zenith angles, resulting in obtain lower P_{cool}. For instance, when T_{amb} is 20 °C, the P_{cool} for the module at solar incident angle of 0° is 85.62 W/m^2, but when the solar incident angle reaches 40°, the corresponding η_{con} drops sharply,

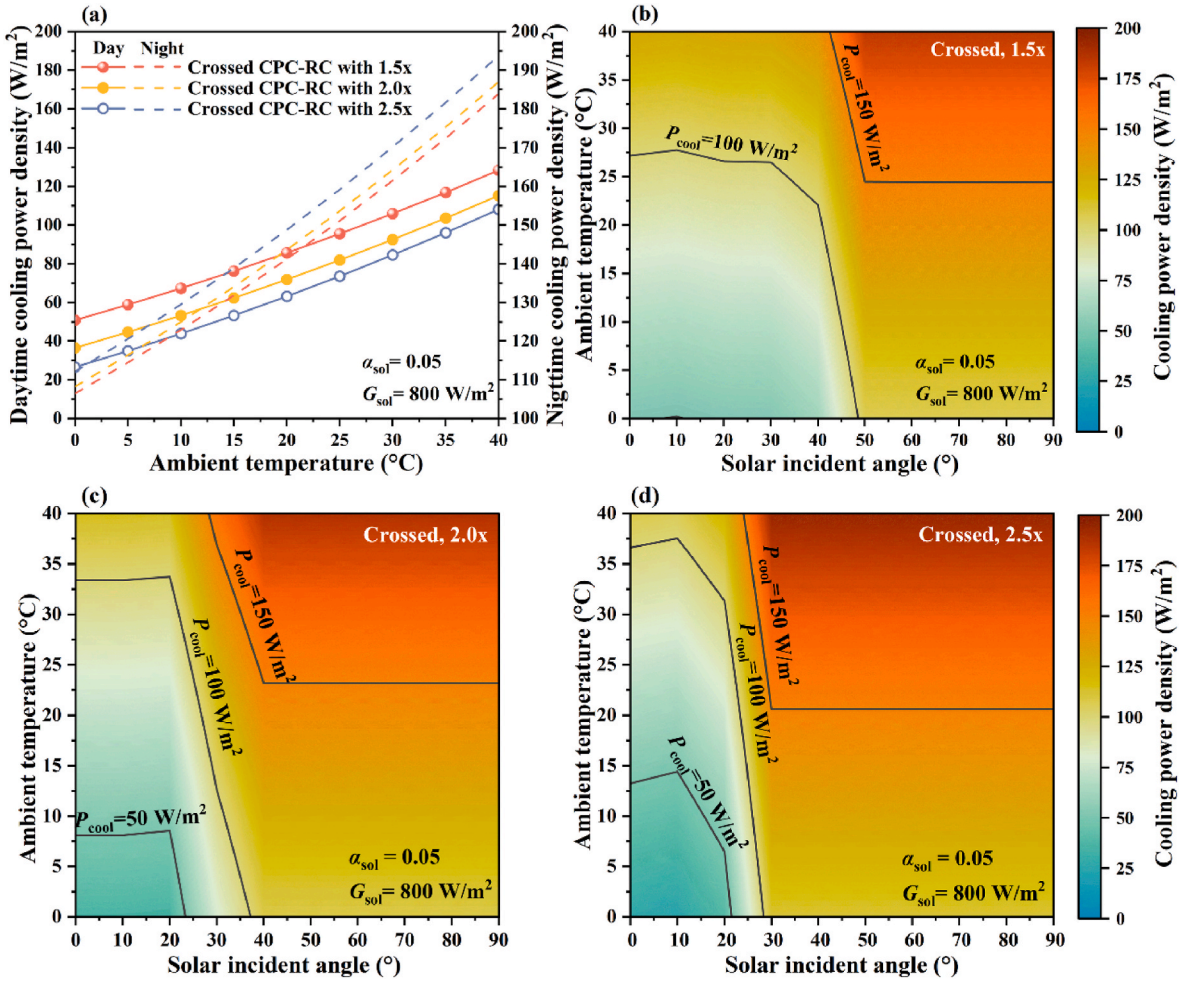

Fig. 14. (a) Cooling performance of the crossed CPC-RC modules with different concentration ratios at different ambient temperatures during the daytime and nighttime. (b), (c) and (d) Cooling power for the crossed CPC-RC module as a function of the solar incident angle and ambient temperature.

Table 3
Solar acceptance ratio for the three crossed CPC-RC modules with different *C*.

	7:00	8:00	9:00	10:00	11:00	12:00	13:00	14:00	15:00	16:00	17:00	18:00
1.5x	0.00	0.00	0.66	0.90	0.93	0.94	0.92	0.90	0.66	0.00	0.00	0.00
2.0x	0.00	0.00	0.00	0.75	0.92	0.93	0.93	0.76	0.00	0.00	0.00	0.00
2.5x	0.00	0.00	0.00	0.03	0.83	0.90	0.83	0.03	0.00	0.00	0.00	0.00

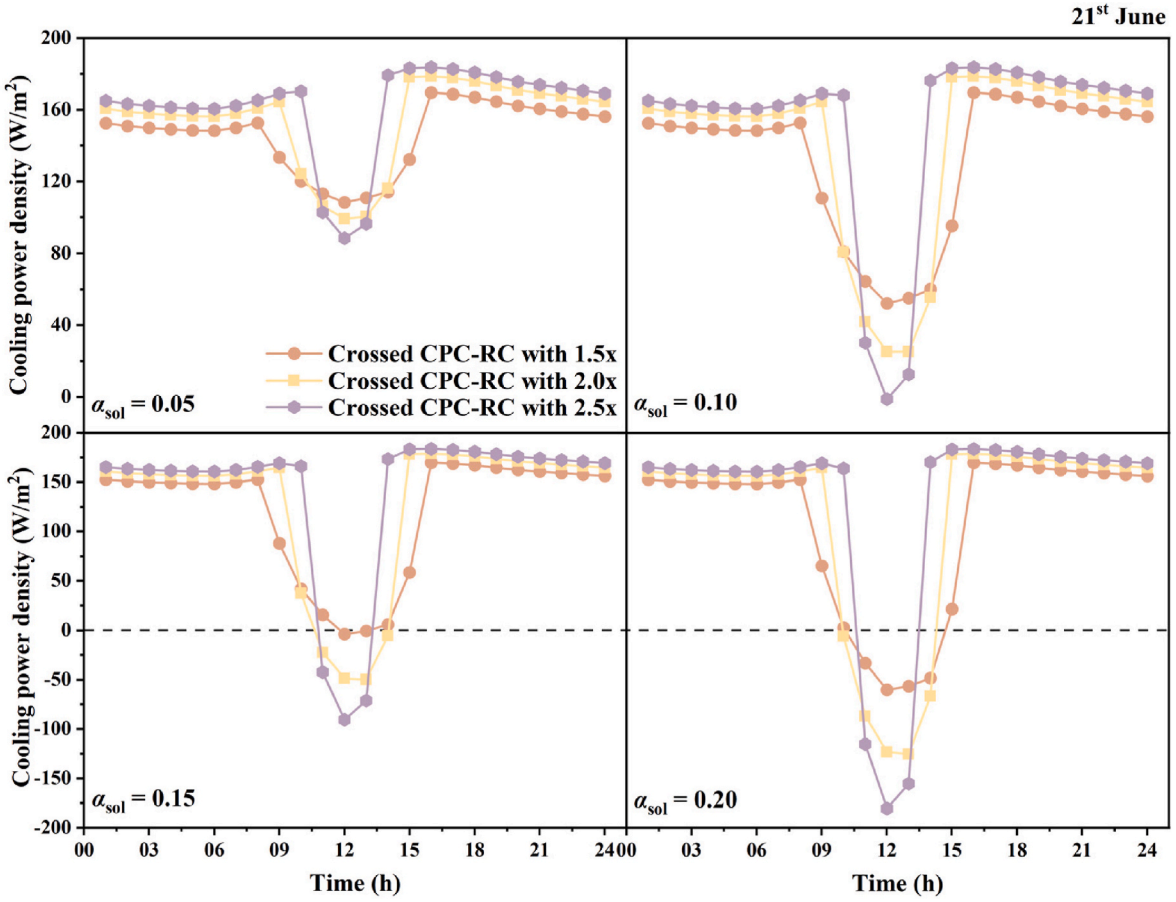

Fig. 15. Hourly cooling power density for the three crossed CPC-RC modules with different RC emitters on 21st June.

causing P_{cool} to rise to 95.89 W/m^2. Moreover, when the solar incident angle exceeds 40°, the crossed CPC structure blocks all solar radiation, causing P_{cool} to increase by 1.47 times compared to when the solar incident angle is 0°, reaching 141.22 W/m^2. When *C* increases, the P_{cool} for the crossed CPC-RC module decreases at small zenith angles due to the increased solar radiation concentrated on the RC emitter. For example, when *C* is 2x, T_{amb} is 20 °C and the solar incident angle is 0°, the P_{cool} for the RC module is only 71.88 W/m^2, compared to 85.62 W/m^2 for the module with 1.5x. This is because, although the CPC structure blocks more external environmental thermal radiation, the increase in *C* causes the module to absorb 28.5% more solar radiation, thereby reducing its cooling performance. However, as the *C* of the crossed CPC-RC module increases, crossed CPC's θ_{max} is smaller, allowing the RC module with a larger *C* to achieve higher P_{cool} when the solar incident angle exceeds the θ_{max}. For instance, when T_{amb} is 20 °C and the solar incident angle is 30°, the P_{cool} for the RC module with 2.5x is 148.78 W/m^2, which is 70.9% and 30.6% higher than the RC modules with 1.5x and 2.0x, respectively.

4.2.2. Cooling performance on a typical summer day

In this subsection, the P_{cool} for the crossed CPC-RC modules with different *C* and RC emitters on 21st June will be discussed. The T_{amb}, T_{sur} and hourly G_{sol} of a typical day are the same as in Section 4.1.

Table 3 shows the η_{con} for the different crossed CPC-RC modules on 21st June. As *C* increases from 1.5x to 2.0x, the crossed CPC structure blocks sunlight for longer, with higher η_{con} observed only around noon (10:00 to 14:00). When *C* reaches 2.5x, it concentrates solar radiation only between 11:00 and 13:00. Additionally, as *C* increases, the η_{con} at noon decreases. For example, the η_{con} for the crossed CPC-RC module with 1.5x at 12:00 is 0.94, while for the RC modules with 2.0x and 2.5x, it drops to 0.93 and 0.90, respectively. This occurs because the crossed CPC-RC module in this section is not truncated and retains its full height, offering better solar-shield performance than the truncated crossed CPC-RC structure described in Section 4.1. However, since the effect of *C* must still be considered, further analysis of the module's final P_{sol} is needed.

Fig. 15 shows the hourly P_{cool} variations of three crossed CPC-RC modules with different *C* on 21st June, with the α_{sol} for the RC emitter changes. The results show that regardless of α_{sol} when the crossed CPC functions as a solar concentrator (i.e., when η_{con} is not 0), a higher *C* results in a lower P_{cool} for the crossed CPC-RC module. Consequently, the P_{cool} for the 2.5x crossed CPC-RC module with 2.5x is the lowest among the three configurations. This occurs because, as the *C* of the crossed CPC-RC module increases, when the solar radiation incident angle is within the θ_{max} of the crossed CPC, more solar radiation will be concentrated onto the RC emitter, which will negatively affect the

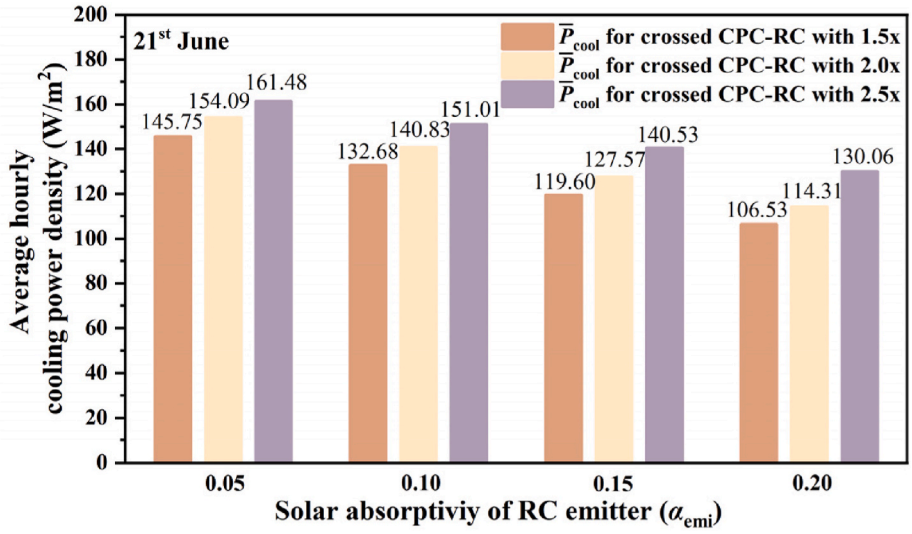

Fig. 16. Average hourly cooling power density for the crossed CPC-RC modules with different RC emitters on 21st June.

cooling performance. Conversely, when solar radiation exceeds the θ_{max}, the module effectively blocks almost all incoming solar radiation. Additionally, as shown in Table 3, the number of hours during which η_{con} for the crossed CPC-RC module with 2.5x larger than 0 is only 3, which is considerably less compared to RC modules with lower C. However, during these 3 h, the absorption of solar radiation is significant. This is because a 2.5x concentrator directs 2.5 times as much solar radiation onto the RC emitter compared to a planar RC module with the same emitter, significantly reducing its cooling performance. For instance, when the α_{sol} for the RC emitter is 0.05, its P_{cool} is only 88.46 W/m^2, which is 10.8% and 18.3% lower than the RC modules with 2.0x and 1.5x at noon, respectively. However, when solar radiation is absent, it achieves the best P_{cool} among the three crossed CPC-RC modules, reaching 165.03 W/m^2 at 1:00, 8.3% higher than the RC module with 1.5x. Furthermore, since its concentration effect is limited to 3 h around noon, further research is needed to evaluate its overall cooling performance throughout the day.

During the period from 11:00 to 13:00, when α_{sol} increases to 0.10, the crossed CPC-RC module with 2.5x cannot achieve a cooling effect, while the P_{cool} for the RC module with 2.0x can obtain 25.11 W/m^2 at noon, though still 51.8% lower than the P_{cool} for the RC module with 1.5x. However, as α_{sol} increased further, none of the three crossed CPC-RC modules can achieve a cooling effect at noon. Fortunately, tilting the crossed CPC-RC module to the anti-sunward side to a certain degree can easily reverse this adverse result, enabling a more efficient and sustained daytime RC effect even at higher α_{sol} values.

Although a larger C in the crossed CPC-RC module may prevent RC from being achieved around noon, the crossed CPC structure could still be advantageous for collecting cooling power over the entire day. This is because it serves as a radiation shield for a longer duration, effectively reducing adverse thermal radiation reaching the RC emitter throughout the day. Fig. 16 shows the $\overline{P}_{cool}$ for the three crossed CPC-RC modules on 21st June. Compared with the $\overline{P}_{cool}$ for different RC modules in Fig. 11, the crossed CPC-RC modules exhibit excellent cooling performance throughout the day, regardless of the changes in C. Furthermore, the larger the C, the higher the $\overline{P}_{cool}$. This is mainly because the crossed CPC structure acts as an adverse radiation shield for a longer duration when C is larger, resulting in more cooling power over the whole day. Even when α_{sol} is 0.20, the $\overline{P}_{cool}$ for the crossed CPC-RC module with 2.5x still reaches 130.06 W/m^2, which is 22.1% higher than the crossed CPC-RC module with 1.5x.

The above results indicate that increasing the C of the crossed CPC-RC module effectively blocks more external environmental thermal radiation and part of solar radiation, thereby enhancing cooling power throughout the day. However, during periods when the solar incident angle is less than the θ_{max} of the crossed CPC, more solar radiation is concentrated on the RC emitter, which negatively impacts cooling performance at these times. Consequently, the appropriate C for the crossed CPC-RC module should be selected based on the local noon solar altitude angle in different geographical locations. For instance, in high-latitude areas like the United Kingdom, where the noon solar altitude angle in summer is approximately 60°, solar radiation would fall outside the θ_{max} of the crossed CPC-RC module, allowing for improved cooling performance with a higher C. Additionally, practical applications often involve integrating novel RC modules into building roofs or facades, needing consideration of factors such as the cost of material and weight of the crossed CPC structure. Previous studies have investigated the weights of crossed CPC structures made from various materials [43], revealing that glass CPC structures weigh almost twice as much as other materials, at approximately 10.41g, making them unsuitable for building applications. Among materials, Topaz plastic weighs only 4.94g, and even when attached with highly reflective aluminium, the weight and cost remain significantly lower than those of glass. However, due to the variability in C and the resulting differences in the height of the crossed CPC structure, the actual weight of the crossed CPC configuration must still be carefully considered.

5. Conclusion

This study proposed a novel RC module integrated with the crossed CPC structure (termed as crossed CPC-RC module) which features a unique configuration capable of shielding more external environmental thermal radiation compared to the traditional 2D CPC-RC module, thereby enhancing overall cooling performance. The paper examines the thermal radiation shielding advantages of the crossed CPC-RC module through numerical analysis and characterizes its net cooling power across various ambient temperatures and CPC configurations. The results indicate that when the ambient temperature is 30 °C during the nighttime, the crossed CPC-RC module blocks 11.7% more external environmental thermal radiation than the flat-RC module, demonstrating its effectiveness in shielding against adverse thermal radiation. However, during the daytime, when the solar incident angle is less than the maximum half-acceptance angle (θ_{max}) of the crossed CPC, the function of CPC changes function as a solar concentrator, reducing its cooling performance. Specifically, at noon on 21st June, the cooling performance of the crossed CPC-RC module is only half of that of that

flat-RC module. Fortunately, the number of hours during which the solar incidence angle is within the θ_{max} of the crossed CPC is relatively small. As a result, the average cooling power of the crossed CPC-RC module is 32.4% higher than that of the flat-RC module on 21st June, showcasing its considerable cooling potential. The paper further investigates the impact of varying concentration ratios (C) of the crossed CPC structure on its cooling efficiency. The findings reveal that although a higher C increases the solar radiation concentrated onto the RC emitter around noon, it also raises the height of the module, enhancing its ability to block external environmental thermal radiation. This results in obtaining higher average cooling power throughout the day. For instance, the crossed CPC-RC module with a 2.5x concentration ratio achieves an average cooling power of 151.01 W/m^2 on 21st June, which is 13.8% greater than that of the module with 1.5x.

Although this paper proposes and validates the ability of the novel crossed CPC-RC module to achieve excellent all-day cooling performance on a typical summer day, it does not investigate the variation in cooling power across different geographic locations and seasons. Since the solar altitude angle changes with these factors, the optimal CPC configurations and deployment orientations will also differ accordingly. Therefore, in future studies, the net radiative cooling power density of the crossed CPC-RC module will be investigated across various geographic locations and seasons to further illustrate its potential for practical applications. Additionally, to simplify the numerical analysis, this study fixed the spectral characteristics of the RC emitter and the size and material properties of the surrounding obstacles. However, when the spectral characteristics of the RC emitter are suboptimal or the ratio of surrounding obstacles increases, the cooling performance of the module is negatively affected. Therefore, future studies will explore the impact of varying these parameters on the cooling performance of the crossed CPC-RC module.

CRediT authorship contribution statement

Ya Dan: Writing – review & editing, Writing – original draft, Software, Investigation, Formal analysis. **Mingke Hu:** Writing – review & editing, Supervision, Methodology, Investigation, Funding acquisition, Formal analysis, Conceptualization. **Qiliang Wang:** Writing – review & editing, Investigation, Formal analysis. **Yuehong Su:** Writing – review & editing, Supervision, Project administration, Funding acquisition, Conceptualization. **Saffa Riffat:** Writing – review & editing, Resources, Project administration.

Declaration of competing interest

The authors declare that they have no known competing financial interests or personal relationships that could have appeared to influence the work reported in this paper.

Acknowledgment

The authors would like to acknowledge the National Natural Science Foundation of China (NSFC 52478107) and the Engineering and Physical Sciences Research Council (Horizon Europe Guarantee grant number: EP/Y016645/1) for the financial support to this study.

References

[1] Ke Li, Lin Boqiang, Impacts of urbanization and industrialization on energy consumption/CO_2 emissions: does the level of development matter? Renew. Sustain. Energy Rev. 52 (2015) 1107–1122, https://doi.org/10.1016/j.rser.2015.07.185.

[2] E. Aramendia, P.E. Brockway, P.G. Taylor, J.B. Norman, Exploring the effects of mineral depletion on renewable energy technologies net energy returns, Energy 290 (2024) 130112, https://doi.org/10.1016/j.energy.2023.130112.

[3] Y. Zhang, M. Hu, Z. Chen, Y. Su, S. Riffat, Performance study of a thermochemical energy storage reactor embedded with a microchannel tube heat exchanger for water heating, J. Energy Storage 78 (2024) 110043, https://doi.org/10.1016/j.est.2023.110043.

[4] Y. Zhu, H. Luo, C. Yang, B. Qin, P. Ghosh, S. Kaur, W. Shen, M. Qiu, P. Belov, Q. Li, Color-preserving passive radiative cooling for an actively temperature-regulated enclosure, Light Sci. Appl. 11 (2022) 122, https://doi.org/10.1038/s41377-022-00810-y.

[5] Y. Liu, Q. Gui, L. Xiao, C. Zheng, Y. Zhang, F. Chen, Photothermal conversion performance based on optimized design of multi-section compound parabolic concentrator, Renew. Energy 209 (2023) 286–297, https://doi.org/10.1016/j.renene.2023.04.002.

[6] G. Wang, Z. Zhang, Z. Chen, Design and performance evaluation of a novel CPV-T system using nano-fluid spectrum filter and with high solar concentrating uniformity, Energy 267 (2023) 126616, https://doi.org/10.1016/j.energy.2023.126616.

[7] Q. Wang, Y. Dan, S. Riffat, H. Yang, Y. Su, M. Hu, Harvesting energy from the sun and space: a versatile collector for simultaneous production of electricity, heat, and cold energy, The Innovation Energy 1 (2024) 100013, https://doi.org/10.59717/j.xinn-energy.2024.100013.

[8] S. Zhao, B. Da, F. Peng, B. Hu, C. Gao, K. Dai, G. Zheng, C. Liu, C. Shen, Facilely fabricated polyethylene film composed of directional microfibrils for passive radiative cooling, Polymer 299 (2024) 126979, https://doi.org/10.1016/j.polymer.2024.126979.

[9] D. Zhao, A. Aili, Y. Zhai, S. Xu, G. Tan, X. Yin, R. Yang, Radiative sky cooling: fundamental principles, materials, and applications, Appl. Phys. Rev. 6 (2019) 021306, https://doi.org/10.1063/1.5087281.

[10] L. Carlosena, Á. Ruiz-Pardo, E.Á. Rodríguez-Jara, M. Santamouris, Worldwide potential of emissive materials based radiative cooling technologies to mitigate urban overheating, Build. Environ. 243 (2023) 110694, https://doi.org/10.1016/j.buildenv.2023.110694.

[11] D. Zhao, A. Aili, Y. Zhai, J. Lu, D. Kidd, G. Tan, X. Yin, R. Yang, Subambient cooling of water: toward real-world applications of daytime radiative cooling, Joule 3 (2019) 111–123, https://doi.org/10.1016/j.joule.2018.10.006.

[12] C.M.S. Kumar, S. Singh, M.K. Gupta, et al., Solar energy: A promising renewable source for meeting energy demand in Indian agriculture applications, Sustain. Energy Technol. Assess. 55 (2023) 102905, https://doi.org/10.1016/j.seta.2022.102905.

[13] H. Ju, S. Lei, F. Wang, D. Yang, J. Ou, A. Amirfazli, Daytime radiative cooling performance and building energy consumption simulation of superhydrophobic calcined kaolin/poly(vinylidene fluoride-co-hexafluoropropylene) coatings, Energy Build. 292 (2023) 113184, https://doi.org/10.1016/j.enbuild.2023.113184.

[14] D. Li, X. Liu, W. Li, Z. Lin, B. Zhu, Z. Li, J. Li, B. Li, S. Fan, J. Xie, J. Zhu, Scalable and hierarchically designed polymer film as a selective thermal emitter for high-performance all-day radiative cooling, Nat. Nanotechnol. 16 (2021) 153–158, https://doi.org/10.1038/s41565-020-00800-4.

[15] H. Sun, F. Tang, Q. Chen, L. Xia, C. Guo, H. Liu, X. Zhao, D. Zhao, L. Huang, J. Li, L. Chen, A recyclable, up-scalable and eco-friendly radiative cooling material for all-day sub-ambient comfort, Chem. Eng. J. 455 (2023) 139786, https://doi.org/10.1016/j.cej.2022.139786.

[16] X. Wu, J. Li, F. Xie, X.-E. Wu, S. Zhao, Q. Jiang, S. Zhang, B. Wang, Y. Li, D. Gao, R. Li, F. Wang, Y. Huang, Y. Zhao, Y. Zhang, W. Li, J. Zhu, R. Zhang, A dual-selective thermal emitter with enhanced subambient radiative cooling performance, Nat. Commun. 15 (2024) 815, https://doi.org/10.1038/s41467-024-45095-4.

[17] Y. Ma, Roll-to-roll printing trench-like metasurface film for radiative cooling, Light Sci. Appl. 12 (2023) 277, https://doi.org/10.1038/s41377-023-01317-w.

[18] Y. Wu, B. Liu, R. Zhang, T. Yu, M. Pu, X. Li, X. Ma, Y. Guo, X. Luo, Temperature-adaptive porous polymer radiative cooling coatings for all-season thermal management and annual energy-saving, Energy Build. 296 (2023) 113423, https://doi.org/10.1016/j.enbuild.2023.113423.

[19] K. Lin, Y. Du, S. Chen, L. Chao, H. Him Lee, T. Chung Ho, Y. Zhu, Y. Zeng, A. Pan, C. Yan Tso, Nanoparticle-polymer hybrid dual-layer coating with broadband solar reflection for high-performance daytime passive radiative cooling, Energy Build. 276 (2022) 112507, https://doi.org/10.1016/j.enbuild.2022.112507.

[20] C.Y. Tso, K.C. Chan, C.Y.H. Chao, A field investigation of passive radiative cooling under Hong Kong's climate, Renew. Energy 106 (2017) 52–61, https://doi.org/10.1016/j.renene.2017.01.018.

[21] I. Haechler, H. Park, G. Schnoering, T. Gulich, M. Rohner, A. Tripathy, A. Milionis, T.M. Schutzius, D. Poulikakos, Exploiting radiative cooling for uninterrupted 24-hour water harvesting from the atmosphere, Sci. Adv. 7 (2021) eabf3978, https://doi.org/10.1126/sciadv.abf3978.

[22] Z. Chen, L. Zhu, A. Raman, S. Fan, Radiative cooling to deep sub-freezing temperatures through a 24-h day–night cycle, Nat. Commun. 7 (2016) 13729, https://doi.org/10.1038/ncomms13729.

[23] E. du M. van Voorthuysen, R. Roes, Blue sky cooling for parabolic trough plants, Energy Proc. 49 (2014) 71–79, https://doi.org/10.1016/j.egypro.2014.03.008.

[24] L. Zhou, H. Song, N. Zhang, J. Rada, M. Singer, H. Zhang, B.S. Ooi, Z. Yu, Q. Gan, Hybrid concentrated radiative cooling and solar heating in a single system, Cell Reports Physical Science 2 (2021) 100338, https://doi.org/10.1016/j.xcrp.2021.100338.

[25] A. Pirvaram, T. Cooper, S.N. Leung, P.G. O'Brien, A comprehensive study on using underside infrared reflectors to enhance the performance of radiative cooling structures, Energy Convers. Manag. 304 (2024) 118180, https://doi.org/10.1016/j.enconman.2024.118180.

[26] B. Zhao, K. Lu, M. Hu, K. Wang, D. Gao, K. Chen, Q. Xuan, G. Pei, Sub-ambient daytime radiative cooling based on continuous sunlight blocking, Sol. Energy

Mater. Sol. Cell. 245 (2022) 111854, https://doi.org/10.1016/j.solmat.2022.111854.
[27] J. Peoples, Y.-W. Hung, X. Li, D. Gallagher, N. Fruehe, M. Pottschmidt, C. Breseman, C. Adams, A. Yuksel, J. Braun, W.T. Horton, X. Ruan, Concentrated radiative cooling, Appl. Energy 310 (2022) 118368, https://doi.org/10.1016/j.apenergy.2021.118368.
[28] Y. Dan, M. Hu, S. Suhendri, Y. Su, S. Riffat, Harnessing the characteristic of compound parabolic concentrators for directional concentration of emitted thermal radiation and solar shielding in building-integrated radiative cooling, Energy Build. 307 (2024) 113922, https://doi.org/10.1016/j.enbuild.2024.113922.
[29] M. Tian, Y. Su, H. Zheng, G. Pei, G. Li, S. Riffat, A review on the recent research progress in the compound parabolic concentrator (CPC) for solar energy applications, Renew. Sustain. Energy Rev. 82 (2018) 1272–1296, https://doi.org/10.1016/j.rser.2017.09.050.
[30] M. Dong, L. Zhu, B. Jiang, S. Fan, Z. Chen, Concentrated radiative cooling and its constraint from reciprocity, Opt Express 30 (2022) 275, https://doi.org/10.1364/OE.445544.
[31] M. Tian, L. Zhang, Y. Su, Q. Xuan, G. Li, H. Lv, An evaluation study of miniature dielectric crossed compound parabolic concentrator (dCCPC) panel as skylights in building energy simulation, Sol. Energy 179 (2019) 264–278, https://doi.org/10.1016/j.solener.2018.12.058.
[32] X. Li, K. Li, Y. Sun, R. Wilson, J. Peng, K. Shanks, T. Mallick, Y. Wu, Comprehensive investigation of a building integrated crossed compound parabolic concentrator photovoltaic window system: thermal, optical and electrical performance, Renew. Energy 223 (2024) 119791, https://doi.org/10.1016/j.renene.2023.119791.
[33] M. Khalid, J. Wei, S. Bakhsh, M.A. Qaisrani, M. Sohail, J. Fang, Comparative optical performance investigation of Cross Compound Parabolic Concentrators designed with the elimination of multiple reflections principle, Sol. Energy 258 (2023) 253–269, https://doi.org/10.1016/j.solener.2023.04.064.
[34] N. Sellami, T.K. Mallick, Optical efficiency study of PV crossed compound parabolic concentrator, Appl. Energy 102 (2013) 868–876, https://doi.org/10.1016/j.apenergy.2012.08.052.
[35] Y. Su, S.B. Riffat, G. Pei, Comparative study on annual solar energy collection of a novel lens-walled compound parabolic concentrator (lens-walled CPC), Sustain. Cities Soc. 4 (2012) 35–40, https://doi.org/10.1016/j.scs.2012.05.001.
[36] L. Evangelisti, C. Guattari, F. Asdrubali, On the sky temperature models and their influence on buildings energy performance: a critical review, Energy Build. 183 (2019) 607–625, https://doi.org/10.1016/j.enbuild.2018.11.037.
[37] Y. Dan, M. Hu, Y. Su, S. Riffat, A generalized modelling approach to performance analysis of radiative sky cooling with complicated configurations and external environments, Renew. Energy 237 (2024) 121729, https://doi.org/10.1016/j.renene.2024.121729.
[38] Y. Dan, M. Hu, Q. Wang, Y. Su, S. Riffat, Comprehensive evaluation of integrating radiative sky cooling with compound parabolic concentrator for cooling flux amplifying, Energy 312 (2024) 133673, https://doi.org/10.1016/j.energy.2024.133673.
[39] Optical Design Software | Photopia | Photopia Optical Design Software, (n.d.). https://www.ltioptics.com/en/optical-design-software-photopia.html (accessed January 31, 2023).
[40] B.M. Marino, N. Muñoz, L.P. Thomas, Calculation of the external surface temperature of a multi-layer wall considering solar radiation effects, Energy Build. 174 (2018) 452–463, https://doi.org/10.1016/j.enbuild.2018.07.008.
[41] IRAM-11601 - Normas Iram - NORMA ARGENTINA 11601 2002 Esta impresiÛn tiene incorporada la - Studocu, (n.d.). https://www.studocu.com/es-ar/document/universidad-nacional-de-catamarca/estructura-de-datos-y-algoritmos/iram-11601-normas-iram/65817854 (accessed November 4, 2024).
[42] J. Torres-Quezada, A. Isalgué, H. Coch, Impact of solar reflectivity and infrared emissivity on the thermal performance of metal and concrete roofs in cloudy warm-humid climate, Frontiers of Architectural Research 13 (2024) 842–857, https://doi.org/10.1016/j.foar.2024.03.003.
[43] K. Shanks, A. Knowles, A. Brierley, H. Baig, H. Orr, Y. Sun, Y. Wu, S. Sundaram, T. Mallick, An experimental analysis of the optical, thermal and power to weight performance of plastic and glass optics with AR coatings for embedded CPV windows, Sol. Energy Mater. Sol. Cell. 200 (2019) 110027, https://doi.org/10.1016/j.solmat.2019.110027.